Applied Ocean Research 138 (2023) 103653

Contents lists available at ScienceDirect

Applied Ocean Research

journal homepage: www.elsevier.com/locate/apor

The wave energy converter control competition (WECCCOMP): Wave energy control algorithms compared in both simulation and tank testing

John V. Ringwood [a,*], Nathan Tom [b], Francesco Ferri [c], Yi-Hsiang Yu [d], Ryan G. Coe [e], Kelley Ruehl [e], Giorgio Bacelli [e], Shuo Shi [f], Ron J. Patton [f], Paolino Tona [g], Guillaume Sabiron [g], Alexis Merigaud [g], Bradley A. Ling [h], Nicolas Faedo [i]

[a] Centre for Ocean Energy Research, Maynooth University, Maynooth, Ireland
[b] National Renewable Energy Laboratory (NREL), Golden, CO, USA
[c] Aalborg University, Aalborg, Denmark
[d] National Yang Ming Chiao Tung University, Taipei, Taiwan
[e] Sandia National Laboratories, Albuquerque, NM, USA
[f] University of Hull, Hull, UK
[g] IFP Energies Nouvelles, Rueil-Malmaison, France
[h] Northwest Energy Innovations, Portland, OR, USA
[i] Marine Offshore Renewable Energy Lab, Politecnico di Torino, Turin, Italy

ARTICLE INFO

Keywords:
Wave energy
Modelling
Control
Estimation
Forecasting
Competition

ABSTRACT

The wave energy control competition established a benchmark problem which was offered as an open challenge to the wave energy system control community. The competition had two stages: In the first stage, competitors used a standard wave energy simulation platform (WEC-Sim) to evaluate their controllers while, in the second stage, competitors were invited to test their controllers in a real-time implementation on a prototype system in a wave tank. The performance function used was based on converted energy across a range of standard sea states, but also included aspects related to economic performance, such as peak/average power, peak force, etc. This paper compares simulated and experimental results and, in particular, examines if the results obtained in a linear system simulation are borne out in reality. Overall, within the scope of the device tested, the range of sea states employed, and the performance metric used, the conclusion is that high-performance WEC controllers work well in practice, with good carry-over from simulation to experimentation. However, the availability of a good WEC mathematical model is deemed to be crucial.

1. Introduction

Energy in ocean waves is distributed across a wide range of frequencies, making it a challenge to minimise the loading on a wave energy converter (WEC) while maximising power capture across the range of sea states that a wave energy installation may be subject to. When using simple resistive damping control, even a well-designed device will fail to capture much of the energy in ocean waves (Hals et al., 2011). As a result, a large number of studies have begun to investigate advanced control design and implementation for WECs; these studies have generally shown encouraging results for increased energy absorption, often accompanied by other desirable characteristics such as decreased loads (Hals et al., 2011; Ferri et al., 2014; Coe et al., 2017), and represent a key path towards lowering the levelised cost of energy (LCoE) for WECs (Neary et al., 2014).

While there are a significant number of studies that evaluate specific WEC devices under particular wave excitation conditions, few studies exist (with the notable exceptions of, for example, Hals et al. (2011), Coe et al. (2017)) which compare a number of control strategies on one (or a set of) standard device(s) with consistent wave excitation applied in each case to level the playing field. In addition, controller evaluations are usually carried out in simulation, where the simulation model is often identical to that used to build the model-based controller. In such a matched situation, any controller sensitivities caused by modelling inaccuracies, such as friction, nonlinearity, and/or viscous

* Corresponding author.
E-mail addresses: john.ringwood@mu.ie (J.V. Ringwood), nathan.tom@nrel.gov (N. Tom), ffer@build.aau.dk (F. Ferri), yyu@nycu.edu.tw (Y. Yu), rcoe@sandia.gov (R.G. Coe), kmruehl@sandia.gov (K. Ruehl), bacell@sandia.gov (G. Bacelli), S.Shi-2016@hull.ac.uk (S. Shi), r.j.patton@hull.ac.uk (R.J. Patton), paolino.tona@ifpen.fr (P. Tona), guillaume.sabiron@ifpen.fr (G. Sabiron), alexis.merigaud@ifpen.fr (A. Merigaud), lingb@azurawave.com (B.A. Ling), nicolas.faedo@polito.it (N. Faedo).

https://doi.org/10.1016/j.apor.2023.103653
Received 23 March 2023; Received in revised form 24 June 2023; Accepted 27 June 2023
Available online 20 July 2023

losses, are masked in the evaluation, but are explored in the second (implementation) phase of the wave energy converter control competition (WECCCOMP). In addition, because of the noncausal nature of optimal impedance-matching control problem (Ringwood et al., 2014), future information (available in simulation environments) (Fusco and Ringwood, 2012) is often assumed for the controller. While there are ways of estimating such future information (Fusco and Ringwood, 2010), the effects of the estimation errors are not always considered (Fusco and Ringwood, 2011).

Despite the fact that some comparative simulation results are available (Coe et al., 2017), there is also a desire to compare a variety of WEC control strategies under real, or at least wave tank, implementation scenarios (see, for example, Nguyen et al. (2016)), so that all real effects are encountered, such as nonlinear hydrodynamic and power take-off (PTO) effects, realistic measurement assumptions, including the presence of measurement noise and/or bias, and real-time computational requirements. In the first (simulation) phase of WECCCOMP, nonlinear power take-off efficiency is included, but remaining effects will be encountered in the second (experimental/implementation) phase of WECCCOMP. Ironically, the control challenge for smaller-scale WECs can be greater due to the exaggerated role of friction and the higher sampling rate requirements associated with faster dynamics, but these issues are, at least, consistent for each of the compared control strategies.

The objective of the WECCCOMP competition, which consists of a standard WEC prototype platform, is to compare the energy capture performance of various WEC control strategies, first in simulation and then, for shortlisted entrants, on the prototype device in a wave tank environment. In order to provide a consistent simulation environment for both competitors and evaluators, the WEC-Sim simulation environment (Ruehl et al., 2014) is employed. For wave tank testing, the real-time control algorithms are implemented using the Matlab/Simulink xPC environment. As a result, we believe that this system, with a standard simulation environment and validated model, standard maintained prototype WEC and PTO system, and connected real-time control computer with a popular programming interface (MATLAB/Simulink), provides an ideal benchmark WEC control platform, with some evidence of its success in this regard documented in Section 10.

The original WECCCOMP parameters were announced in Ringwood et al. (2017), with the results from the simulation stage of the competition subsequently presented in Ringwood et al. (2019). This paper now documents the comparative results from the experimental stage of the competition, where competitors were assigned 2.5 days each to implement their control and produce a standard set of control results, funded by the Marinet 2 programme, at the Aalborg University Wave Basin. In particular, there is significant interest in the examination of any degradation of results in the move from the somewhat ideal simulation environment to the more realistic experimental platform. The paper does contain some overlap with the results presented in Ringwood et al. (2019); however, the authors believe this is important in the comparative analysis of simulation and tank test results, which was one of the objectives of WECCCOMP. Some further information on WECCCOMP is available at https://coer.maynoothuniversity.ie/wec-control-competition-released/.

The remainder of the paper is laid out as follows: Section 2 describes the experimental system under study and briefly reviews the hydrodynamic model. The performance criteria used in WECCCOMP are introduced in Section 3, while the simulation and implementation environments are documented in Sections 4 and 5, respectively. An overview of each of the specific control solutions is given in Sections 6 to 8, with further details of each of these algorithms given in the dedicated (Ling, 2019), Shi et al. (2019), and Tona et al. (2020), respectively. Comparative simulation and implementation results are given in Section 9, including a technical comparison of the 3 controller algorithms, with conclusions drawn in Section 10.

2. The prototype WEC system

The system to be used in the control competition is a single degree of freedom (DOF) WEC (see Fig. 2), based on a segment of the WaveStar WEC (Bjerrum, 2008). Though, hydrodynamically, there are multiple DOFs of the conventional coordinate system, which includes surge, heave, and pitch, these are not independent and are resolved into a single mechanical PTO DOF, namely rotation (θ, $\dot{\theta}$) around point A. The mechanical rotation at A is subsequently translated into linear motion of the arm connecting B and C, and ultimately into electrical power via the linear generator/motor (indicated in Fig. 2). Note that the linear actuator can both absorb power (generation) as well as providing for reactive power into to the WEC (motoring). At equilibrium, the floater arm stands at approximately 30° with respect to the water line. The submerged volume of the floater resembles a hemisphere in the static position. Additional annotation in Fig. 2 includes the mounting frame, which is suspended from a fixed gantry over the wave tank (which has minimal motion), $\eta(x,t)$ describes the free surface elevation in space and time (see Eq. (1)), while SWL denotes the still water level. An accelerometer provides a specific measurement of the floater motion, if required.

The system is equipped with the following hardware:

Linear Motor and Controller – LinMot Series P01-37x240F and LinMot E1200
Force Sensor – S-beam load cell, Futek LSB302 300lb, with SGA Analogue Strain Gauge Amplifier
Position Sensor – MicroEpsilon ILD-1402-600
Accelerometer - Dual-axis accelerometer, Analog Devices ADXL 203EB
I/O Board – DAQ NI PCI-6221 DAQ

Additionally, real-time information about sea surface elevation at three separate points up-wave of the floater are provided using resistive wave gauges. The position of these gauges, along with other details of the tank dimensions and layout, are shown in Fig. 1. In terms of wave generation, the desired wave spectrum is discretised, yielding approx. 1500 frequency bins and the phases of individual components are randomised, but a consistent wave train can be achieved by using a fixed seed value. Second-order wave theory is used to calculate paddle motion (paddles are force controlled, giving active absorption), with a sampling frequency of 50 Hz, with typical run times of 300 s.

The linear motor (PTO system) can be driven either as a force or position follower. For the case of the force follower, the target force can include a reactive power term. While the actuator is rated up to ±200 N, the force provided by the actuator is constrained to the more realistic range of ±60 N, with this limit becoming active for more energetic sea states. Relevant dimensions and mechanical properties of the system are listed in Table 1. Note that the linearly measured position and force are accurately converted into the angular motion of the WEC and the control moment, respectively, through a nonlinear trigonometric calculation.

Hydrodynamic model

The floater–wave interaction is essentially modelled by a linear hydrodynamic model:

$$\begin{aligned}(M+m_\infty)\dot{v}(t)+\int_0^{+\infty}h_r(\tau)v(t-\tau)d\tau+K_b x(t)\\ +C_d v(t)=\int_{-\infty}^{t}h_{ex}(\tau)\eta(t-\tau)d\tau+F_{PTO}.\end{aligned} \tag{1}$$

where m_∞ is the added mass at infinite frequency, K_b is the restoring force stiffness, η is the free surface elevation, measured at the location of the floater, and $v(t)$ is the WEC heave velocity, referred to point E in Fig. 2. The non-parametric hydrodynamic quantities $h_{ex}(t)$ and

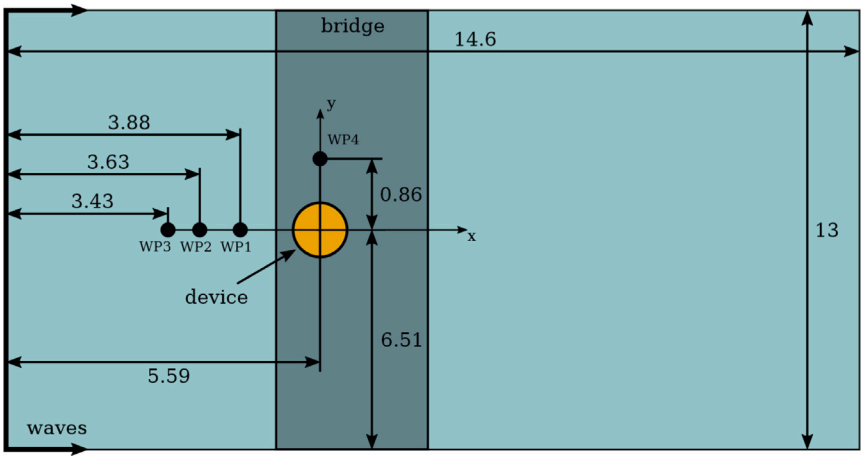

Fig. 1. Schematic of wave tank used for experimental testing, showing the relative position of the device floater (in yellow) and the wave probes (WP1–WP4). Dimensions are in metres.

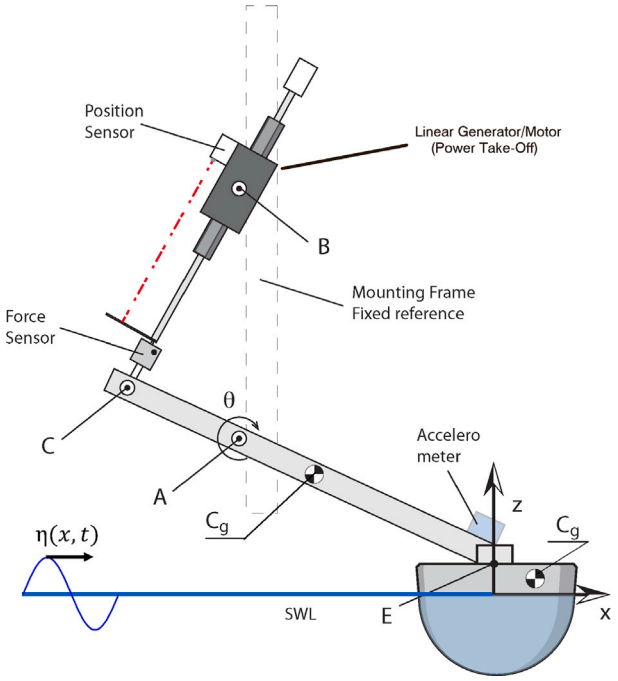

Fig. 2. Schematic of experimental WEC system with the dimensions listed in Table 1.

Table 1
WAVESTAR 1/20 scale model dimensions and mass properties relative to still water line origin.

Parameter	Value [unit]
Float mass	3.075 [kg]
Float Cg (x, z)	(0.051, 0.053) [m]
Float MoI (at Cg)	0.001450 [kg m^2]
Float draft	0.11 [m]
Float diameter (at SWL)	0.256 [m]
Arm mass	1.157 [kg]
Arm Cg (x, z)	(−0.330, 0.255) [m]
Arm MoI (at Cg)	0.0606 [kg m^2]
Hinge A (x, z)	(−0.438, 0.302) [m]
Hinge B (x, z)	(−0.438, 0.714) [m]
Hinge C (x, z)	(−0.621, 0.382) [m]

$h_r(t)$, representing the excitation force and radiation damping dynamics respectively, are calculated numerically using the linear boundary-element potential solver WAMIT (Lee and Newman, 2016). Eq. (1) represents the venerated Cummins' equation, but with the addition of a linear viscous drag term, with coefficient C_d. Note that F_{PTO} is the mechanical force applied by the PTO system, via the linear motor/generator, calculated by the control algorithm employed.

The model has been validated against tank test data, with detailed validation results reported in Ringwood et al. (2017), Tom et al. (2018). The hydrodynamic boundary element method (BEM) solution obtained from WAMIT was provided to the contestants to limit discrepancies between competitor numerical models. This is required, in particular, for the simulation phase of the competition. For the experimental phase, competitors are also given the opportunity to use some of their tank testing time (total of 2.5 days per competitor) to tune the system model, or apply system identification techniques to data recorded from the system as part of their tests.

3. Evaluation criteria

The basis for the evaluation criterion considers the following variables:

1. **Average extracted power**
2. **Capacity factor** – Peak power (95th percentile) over RMS.
3. **Peak PTO force** – The 95th percentile of PTO force
4. **PTO utilisation factor** – Ratio of peak PTO force and RMS PTO force

Based on further consideration, the evaluation metric was updated from its original format in Ringwood et al. (2017) to the following evaluation criterion (EC):

$$EC = \frac{\text{avg}\,(P)}{2 + \frac{|f|_{98}}{F_{max}} + \frac{|z|_{98}}{Z_{max}} - \frac{\text{avg}|P|}{|P|_{98}}} \tag{2}$$

where $|f|_{98}$ is the 98th percentile of the absolute motor force time history (in N), F_{max} is the motor force constraint on the PTO (60 N), $|z|_{98}$ is the 98th percentile of the absolute motor displacement time history (in m), Z_{max} is the motor displacement constraint on the PTO (0.08 m), avg$|P|$ is the mean absolute electrical power (in W), and $|P|_{98}$ is the 98th percentile of the absolute power time history (in W).

The goal of the developed control systems is to *maximise* the EC, which acts as a benefit-to-cost ratio. Specifically, (2) can be considered as a surrogate for LCoE, with the numerator articulating average power produced (directly related to energy), with each of the denominator terms representing system constraints (related to capital costs) in force (F_{max}) and displacement (Z_{max}), while $\frac{\text{avg}|P|}{|P|_{98}}$, represents average-to-peak power, being a positive contribution (peak-to-average is, of course, a cost). The constant 2 in the denominator is to scale the

Table 2
Evaluation sea states.

Sea state	H_s [m]	T_p [s]	γ	P_w [W/m]
SS1	0.0208	0.988	1	0.182
SS2	0.0625	1.412	1	2.556
SS3	0.1042	1.836	1	9.390
SS4	0.0208	0.988	3.3	0.192
SS5	0.0625	1.412	3.3	2.735
SS6	0.1042	1.836	3.3	10.00

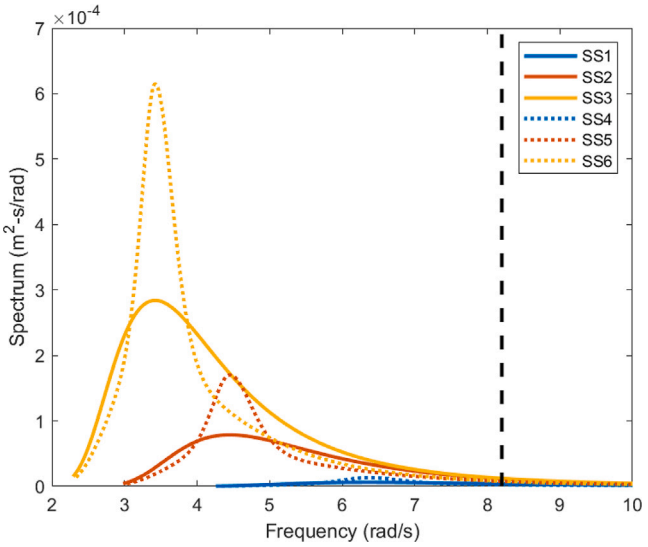

Fig. 3. Wave spectra for the sea states used in controller evaluation, and the float heave resonance frequency (black dashed line).

EC appropriately. While Eq. (2) does not represent a direct measure of LCoE, it is an attempt to approximate related LCoE components at a very high level, but could not be used to ascertain commercial viability of a full-scale WEC system. Rather, the EC is more tuned to examine various aspects of control performance, in terms of positive contributions (average power, average-to-peak ratio) and negative contributions (potential constraint exceedance). Note that the physical constraints, F_{max} and Z_{max}, are not rigidly enforced in the simulation evaluation. In fact, F_{max} and Z_{max} can be exceeded in simulation and, to some extent, in implementation. Rather, their relativity to $|f|_{98}|$ and $|z|_{98}$ (respectively) are captured in the EC. This approach was chosen to avoid a situation in which both of the constraints cannot be simultaneously satisfied.

A total of six sea states were selected to evaluate the controllers (see Table 2). These sea states were selected based on their energy content relative to the response of the scale WaveStar WEC. The wave spectra for the sea states are plotted along with the device heave natural resonance frequency in Fig. 3. Note the disparity between the sea spectral peaks and the natural device resonant frequency, chosen deliberately in order to exercise the controllers. While the energetic sea states (e.g. SS3 and SS6) will exercise the ability of the controllers to handle physical system constraints, the benign sea states (e.g. SS1 and SS2) will present challenges in handling a relatively low signal/noise ratio (SNR), particularly in the experimental setup.

4. WEC system simulation

For the simulation stage of WECCCOMP, a model of the Wavestar device with control was implemented in WEC-Sim. WEC-Sim is an open-source code jointly developed by Sandia National Laboratories and the National Renewable Energy Laboratory, through funding from the U.S. Department of Energy's Water Power Technologies Office (WEC-Sim, 2018). The WEC-Sim code is developed in MATLAB/Simulink, and uses Simscape Multibody to solve for a WEC's rigid body dynamics. WEC-Sim's implementation is a collection of MATLAB scripts (*.*m* files) and Simulink libraries (*.*slx* files), which are hosted on an open-source GitHub repository (WEC-Sim-Github, 2018), with v4.0 released in September 2019.

WEC-Sim is a time-domain code that solves for the system dynamics of WECs consisting of a combination of rigid bodies, PTO systems, mooring systems, and control systems. The dynamic response in WEC-Sim is calculated by solving the WEC's equation of motion for each rigid body about its centre of gravity, in 6 DOFs, based on Cummins' formulation (Cummins, 1962).

The WEC-Sim source code includes a preprocessing BEM input/output code that imports hydrodynamic data generated by the potential flow solvers WAMIT, NEMOH, or AQWA, and parses the BEM data into a (*.*h5*) data structure that is read by WEC-Sim. For more information about WEC-Sim theory, implementation, functionality, and application, refer to the WEC-Sim website (WEC-Sim, 2018). In relation to sea state realisation, 499 bins of equal energy are selected that are added together in a multi-sine and given random phases. The contestants were instructed to use a constant phase seed for each sea state and was used to run the competitors controller so the same wave elevation was used in the evaluation.

A WEC-Sim model of the Wavestar device is described in Tom et al. (2018) to represent the physical Wavestar model that will be tested during the experimental stage of WECCCOMP. The numerical model includes the float's hydrodynamic response as well as the physical inertia of linkages and bearings. The WEC-Sim Simulink model includes the float as a hydrodynamic body block. The connection between the float and arm is a fixed connection. Similarly, revolute joints A, B, and C are modelled by revolute constraints in WEC-Sim. The WEC's non-hydrodynamic bodies consist of the following: arm, frame, Rod BC, and motor linear actuator mass. The movement of Rod BC is modelled by a translational PTO (linear motor), which is actuated based on the control algorithm written in the competitor's controller block. The WECCCOMP controller may use inputs from the upstream wave gauge(s) and either the linear force and displacement of the motor, or the rotary torque and displacement of the float. The numerical model of the Wavestar device was provided to WECCCOMP contestants for development of their controller through a GitHub repository (WECCCOMPGithub, 2018). In addition, the hydrodynamic BEM solution obtained from WAMIT (Lee and Newman, 2016) was provided to the contestants to limit discrepancies between competitor numerical models. Details on the validation of the numerical WEC-Sim model against experimental results from wave tank tests are provided in Tom et al. (2018).

5. Implementation environment

The main objective of the control competition is to test, verify, and calibrate control algorithms on the prototype hardware, for the control objective documented in Section 3. To achieve this objective, a rapid control prototyping (RCP) architecture is used, which facilitates the importation of a controller, which has been tested in a numerical environment, into a real-time operating system connected to a real-world input/output interface. This step is of paramount importance, since any numerical model is only an approximation of the corresponding real-world system.

The RCP architecture is implemented in the Matlab/Simulink (version R2015b) environment, using the xPC Target toolbox, with the RCP architecture sketched in Fig. 4. The hardware WEC comprises sensors, floater, mechanical and structural elements, linear actuator and related controllers. The WEC is interfaced to the Target PC via an I/O board. The Target PC runs a hard real-time operating system (OS) and embeds the controller under development. The base target PC sample frequency is 1 kHz, while the controller sample frequency

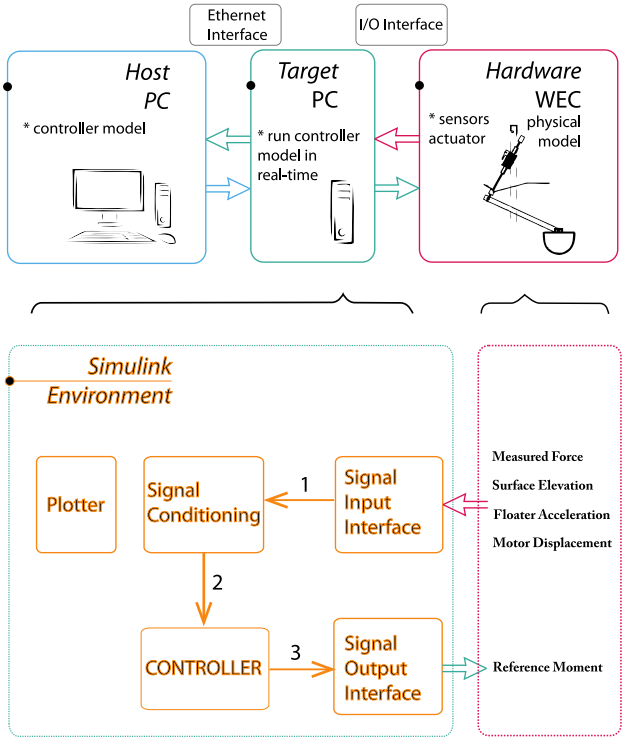

Fig. 4. Top: Simplified block diagram of the Simulink xPc target Rapid Control Prototyping Architecture. Bottom: High-level Simulink development environment.

depends upon the computational cost of the controller itself, e.g. a simple linear damping control can run as high as 1 kHz. Nevertheless, it should be noted that the sampling frequency of the controller must be an integer divider of the base sampling frequency in the Target PC.

The Target and Host PCs communicate through a local intranet connection. The controller under development is implemented in the Host PC, using a Simulink block diagram and then deployed on the Target PC as a compiled code segment. Once running, the controller parameters are accessible (modifiable) from the Host PC.

The lower part of Fig. 4 represents the high-level Simulink block diagram. The measurements from the hardware are collected (line 1) and sent through the signal conditioning block. Line 1 comprises the linear motor rod relative position, the force balance at the load cell, the linear acceleration of the floater, and the wave gauges signals; all the signals are in volts. Within the signal conditioning block, calibration functions, geometric transformations, and LP filters are applied. A state observer is used to retrieve information about system velocity. The output signal (line 2) comprises angular displacement, velocity and acceleration, moment and water elevation at the measurement point; all the rotation and moments are given with respect to the pivoting point A. Line 2 represent the input to the CONTROLLER block, where the control algorithm provided by the WECCCOMP competitor is implemented. The output of the CONTROLLER block (line 3) is the force/position used as reference for the internal force/position control loop within the signal output interface block. For sake of simplicity, the interface of the controller block is summarised in Table 3

It is important to note that not all the Simulink libraries and Matlab functions are compatible with the xPC toolbox, due to limitations in the compiler engines; a list of supported toolboxes and functions can be found in the Matlab-R2015b documentation or at https://se.mathworks.com/products/compiler/supported/compiler_support.html. This provided a few surprises, with limited opportunity for reworking code in the narrow implementation time window, and could have led to (unquantified) disparities between controller implementations in simulation and tank tests.

Table 3
Controller interface definition.

Signal	Unit
Input	
Angular displacement	rad
Angular velocity	rad/s
Angular acceleration	rad/s^2
Resultant moment	N m
Surface elevation at the selected location(s)	m
Output (either Moment or Position)	
Reference Moment	N m
Reference Position	rad

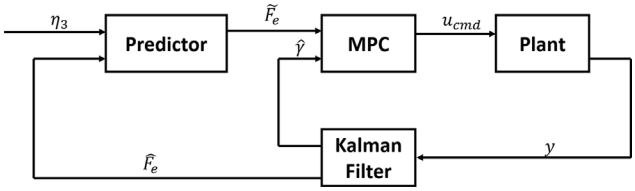

Fig. 5. Block diagram of Bradley Ling's control system.

6. Control solution – Bradley Ling (C1)

6.1. Controller development

Bradley Ling developed a linear model predictive controller for the competition. A block diagram of the control design is shown in Fig. 5. This subsection provides a brief overview of the control design; for additional detail and simulation results, readers are referred to Ling (2019).

The controller utilises a linear state space model of the WEC, full state feedback and a short-term prediction of future excitation forces to determine the control force at each time step that will optimise the objective function. The objective function is chosen as a linear combination of mechanical power and control force squared, a necessary term to ensure convexity of the quadratic problem. The controller can incorporate system constraints into the optimisation problem; in this case, limits were placed on the maximum absolute PTO force and maximum absolute PTO displacement. This MPC framework is not a novel control approach for a WEC; very similar approaches have been extensively studied (e.g. Ling et al. (2019), Starrett et al. (2015), Brekken (2011)). This control design is therefore representative of a typical predictive WEC control design. However, every new control design requires slightly different design decisions, based on the sensors and actuators available. The control design detailed in Ling (2019) was designed with the specific objective of applying a standard WEC MPC framework to the competition, and to utilise the available sensors and inputs to maximise the average evaluation criteria score for the six evaluation sea states. The control design includes three primary components, an MPC controller, an estimator, and a predictor. A brief summary of each component is given in the following paragraphs.

The MPC controller relies on having an accurate state space model of the WEC. This model was developed by applying system identification techniques to the step response of the WEC-Sim model. This linear state space model becomes

$$\dot{\zeta} = A\zeta + Bu \tag{3}$$

$$\dot{x} = C\zeta + Du, \tag{4}$$

where u is PTO torque, $\dot{x}$ is rotational velocity of the float, ζ is the state vector, and A, B, C, and D are the state space matrices derived from the system identification process. The MPC implementation is a standard formulation for wave energy applications; readers are referred to Ling (2019) for more detail.

The short-term excitation force prediction is generated using a linear autoregressive model with exogenous inputs. Linear autoregressive models have been previously proposed to apply MPC to WECs (Ling and Batten, 2015; Brekken, 2011; Fusco and Ringwood, 2010); the approach presented here adds recent prior up-wave water surface elevations as exogenous inputs to the prediction model. Inclusion of the up-wave measurements as additional exogenous inputs to the prediction model significantly improves the prediction accuracy for a time horizon for up to 3 s. The inputs to the prediction model are the estimated excitation force from the Kalman filter and the measured water surface elevation from one of the up-wave sensors. This excitation force prediction model for time t is given, in matrix form, as

$$\begin{bmatrix} \tilde{F}_e(t+N*dt) \\ \vdots \\ \tilde{F}_e(t+dt) \end{bmatrix} = \begin{bmatrix} \beta_{1,1} & \cdots & \beta_{1,2M} \\ \vdots & \ddots & \\ \beta_{N,1} & & \beta_{N,2M} \end{bmatrix} \begin{bmatrix} \eta_3(t) \\ \vdots \\ \eta_3(t-(M-1)*dt) \\ \hat{F}_e(t) \\ \vdots \\ \hat{F}_e(t-(M-1)*dt) \end{bmatrix}, \tag{5}$$

where dt is the time step of the predictor, $\hat{F}_e$ is the estimated excitation force, $\beta_{i,j}$ are the linear regression coefficients, η_3 is the measured up-wave water surface elevation, and $\tilde{F}_e$ is the predicted excitation force. The coefficient matrix $\boldsymbol{\beta}$ can be calculated by using a least-squares fit for previously recorded $\hat{F}_e$, η_3, and $\tilde{F}_e$ values. The fit is applied independently for each prediction horizon time step, resulting in N least-squares fits to determine each row of the $\boldsymbol{\beta}$ matrix. In the simulation evaluation phase, this is straightforward to do, as all values are accessible from the WEC-Sim model. For the experimental implementation, the process to estimate the $\boldsymbol{\beta}$ matrix is described in the next subsection.

6.2. Experimental testing

The first step of experimental testing was to run some simple system identification tests. Step inputs of various magnitudes were applied to the motor, in the absence of wave excitation. Results from these tests were utilised to ensure the data acquisition system and motor control were operating as expected.

Next, a series of damping control tests were run. A PTO force proportional to PTO velocity was applied for all wave cases. This served two purposes:

(a) To provide a performance baseline to compare MPC results to, and
(b) For use in tuning the estimation and wave prediction algorithms.

The damping coefficients for each wave case were selected to maximise power output for each wave case, based on WEC-Sim simulations performed prior to the test.

Excitation force tests were performed on a subset of the sea states. These tests were performed by mechanically restricting the motion of the WEC. The resulting force measured by the load transducer is the excitation force. The results of these tests were used to provide a 'true' excitation force that could be used to tune the estimator and predictor models.

The process and measurement covariance matrices used in the Kalman Filter were then tuned offline. This process was performed by using the experimental measurements as inputs to the filter, and comparing the estimated excitation force values to the experimental excitation force data from the excitation tests. The covariance matrices were adjusted until the difference between the estimated and measured excitation force was acceptable.

The prediction model was tuned using the estimated excitation force from the experimental damping tests ($\hat{F}_e$), and the up-wave elevation (η_3), as inputs. The target excitation forces ($\tilde{F}_e$) used in the least-squares regression are the estimated excitation forces from the experimental (free response) damping tests. This process is non-causal; it requires knowledge of the future estimated excitation force. But, since this process is performed offline, rather than in real-time, this is not a problem. The final prediction model is static, i.e. the $\boldsymbol{\beta}$ matrix is not updated as new data are collected.

Once the state space model, estimator, and prediction model were updated with the wave tank results, some limited tuning of the controller was performed. The primary focus of this tuning was to validate the controller was behaving as expected, and identify any inconsistencies in the implementation of the algorithm in the hardware. Once this debugging step was completed, the final tests for all sea states and realisations were run. The control parameters were held constant for all sea states.

The experimental results closely matched the simulation results; the average EC score over all the wave cases was 2.1% lower in the experimental results compared to the submitted simulation results.

As the first team to perform the wave tank testing, time constraints limited the amount of tuning that could be performed on the controller. Some of the already limited testing time was used to validate and debug the motor control and instrumentation. If more experimental time would have been available, this competitor would have used the extra time to run additional cases to tune the PTO torque limits and to run additional system identification tests to improve the accuracy of the state space model used in the MPC.

7. Control solution – Univ. of Hull (C2)

7.1. Controller development

The control strategy used in this competition is a prediction-less suboptimal causal controller, which does not assume an accurate model or perfect wave excitation force prediction. The performance depends on the choice of mass–spring-damping coefficients of the proposed causal controller, hence the form of the controller is the same as a time-varying PID controller. A Bayesian optimisation (BO) algorithm is adopted to determine the optimal coefficients of the causal controller for each of the prescribed sea states. The BO approach learns the optimal coefficients efficiently in a short period with only several dozen trials. The fast-learning and model-free capabilities make the proposed strategy simple and easy to implement in the real application system.

The concept of the proposed approach is inspired by complex-conjugate control and causal realisation of the non-causality. It is well known that the optimality of complex-conjugate control is strictly limited to monochromatic waves. To achieve the optimal performance under polychromatic wave conditions, a second-order controller can be used as follows (Bacelli et al., 2019):

$$F_{pto}(s) = \frac{M_{pto}s^2 + B_{pto}s + C_{pto}}{s^2 + a_1 s + a_0}\dot{X}(s), \tag{6}$$

where M_{pto}, B_{pto}, C_{pto}, a_1 and a_0 are coefficients, F_{pto} and $\dot{X}(s)$ are the Laplace transform of the PTO force and buoy pitching velocity, respectively.

Although this second-order controller is still a suboptimal causal control system, its response can almost perfectly match the optimal response over a full range of sea state frequencies. This demonstrates the near-optimal potential of the causal controller, which is not prediction-dependent. However, this representation may suffer from poor stability margins since the gain increases rapidly with increasing frequency. Furthermore, determination of the safe exploration range of these coefficients is a non-trivial task. When the considered sea states of a WEC correspond to relatively narrow-banded frequency operation, the performance of the simpler spring–mass–damper control presents little difference compared with other optimal controllers. The proposed prediction-less and model-free suboptimal causal controller is potentially competitive, especially when taking into account the prediction inaccuracy (Shi et al., 2018) and modelling bias that accompanies typical optimal non-causal control approaches. Hence, a PID controller,

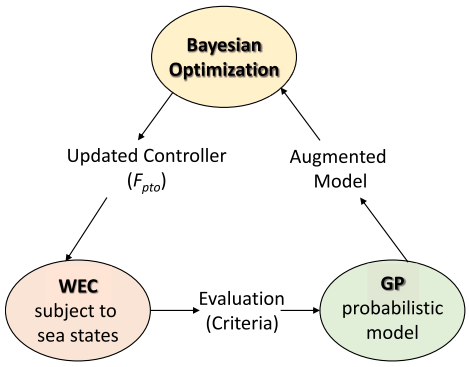

Fig. 6. Hull control system.

corresponding to the spring–mass–damper controller, is chosen for this competition.

The optimal coefficients of the PID controller are learned in real time through the BO procedure during real-time operation, which is depicted in Fig. 6.

The BO adopts a probabilistic Gaussian process (GP) model to approximate the relationship between the controller coefficients and controller performance, which is evaluated by the transformed criteria (Shi et al., 2019) used in this competition. The controller coefficients are updated through the acquisition function, which uses the mean and variance information provided by the GP model, to automatically make a trade-off between exploration and exploitation. Hence, only a few evaluations are required to find the optimal settings by searching and fitting within the promising regions, rather than exploring all possible combinations.

7.2. Estimator development

A robust unknown input observer was developed (Abdelrahman and Patton, 2019) for estimating the wave excitation force for each sea state. This was designed to obtain the wave elevation. However, this estimation strategy was not adopted in the tank experiment due to the availability of the wave gauges but was used in the first stage of the competition. The criterion score is transformed into a relatively constant value for the same controller coefficients in the same sea state, otherwise the BO can be confused by different evaluation results for the same inputs (Shi et al., 2019).

7.3. Controller tuning

Unlike the other chosen MPC methods, this control strategy is a model-free learning method, and the controller coefficients can only be learned during the tank test for each sea state. Hence, the proposed method is relatively time-consuming at the application campaign stage, even though it is already very data efficient. In the experiment, the controller coefficients were updated approximately every 40 wave periods and nearly 30 iterations were required to complete the optimisation, i.e. at least 30 min were needed to determine the optimal coefficients for one sea state. The 2.5 experimental days were organised into three stages, as follows. It took almost one day to become familiar with the hardware environment and compile the algorithm as well as confirming that recognition well on the target system. The second day was used to implement the on-line learning optimisation to determine the optimal coefficients for the six sea states. The last half-day was used to evaluate the coefficients to check that all the required experimental procedures were met. Mindful of the integrity of the experimental hardware, the larger damping values are provided as the lower bound for the BO. The damping term can only affect the optimal amplitude condition while the optimal phase condition is still satisfied. However, there was no second opportunity to reset this value due to the limited experimental time. The learning rate coefficients in the acquisition function and the coefficient in the transformed criterion were again selected from the simulation results, due to the limited time available for the actual experimental campaign (Shi et al., 2019). Therefore, the resulting controller performance was relatively conservative.

Most of the time at the tank test campaign was spent on the development of the filter and observer to deal with excessively noisy acceleration measurements; this proved to be the biggest bottleneck and hurdle impeding the progress and limiting the performance of the controller. In the proposed controller, the sum of the mass, damping and spring terms yields the PTO force; thus, the noisy acceleration measurements had a very significant effect, giving rise to a noisy PTO force signal. The resulting high-frequency components in the PTO force lead to some wasted energy consumption and unstable performance. This, in turn, impeded the convergence of the optimisation algorithm. Although the issue was partially resolved, the noisy acceleration measurements had a detrimental effect on the control performance in the tank experiment. In effect, the noisy acceleration signal makes the performance of the spring–mass-damping controller comparable with or even less than the simple spring-damping controller, which is only optimal for regular waves. For the small wave conditions, there is net energy consumption (rather than generation), likely due to mismatch between the model used by the controller and the real system.

The computation of the six groups of controller coefficients within a short experimental duration had to be done in haste and, consequently, the potential of the proposed approach was not fully realised. However, the performance of the proposed suboptimal control strategy could be competitive against other optimal methods in practice, especially when all the tunable parameters are well computed and assuming that an anti-noisy technique is well designed. This latter step could have been done with foresight that the acceleration measurement was unfiltered.

8. Control solution – IFPEN (C3)

8.1. Controller development

IFPEN model predictive control (MPC) system (Nguyen et al., 2016) is sketched in Fig. 7.

At its core, a weighted-QP model predictive control (wQP-MPC) algorithm maximises the average electric power output avg(P) using wave moment predictions over a given horizon. While simple, the PTO efficiency law used to compute avg(P) is nonlinear, and taking it into account generally leads to a non-convex criterion, the optimisation of which may prove difficult in real time, due to computational constraints. One of the key features of the IFPEN algorithm is the introduction of an equivalent discrete objective function where the instantaneous mechanical power values are weighted over the prediction horizon. The weightings are chosen offline using an iterative optimisation procedure (via a Nelder–Mead algorithm) based on repeated simulations of the nominal model used for MPC design over a set of sea states. This way, the complexity of maximising the original non-convex criterion is shifted to an offline optimisation procedure, which is not subject to real-time computational constraints, while a convex QP-problem is solved online. For WECCCOMP, with respect to the approach in Nguyen et al. (2016), a second offline optimisation step for the MPC controller was added in order to find a local maximum for the evaluation criterion (which is not purely energetic) in the vicinity of the optimal solution, which maximises electric energy production for the selected sea states. The design model for wQP-MPC is a linear state-space realisation derived from Cummins' equation (Cummins, 1962), with wave excitation moment and PTO moment as inputs and float rotational velocity and displacement as outputs. If PTO low-level control is sufficiently fast, its dynamics can be neglected in the wQP-MPC design. Otherwise, it is possible to include it in the repeated

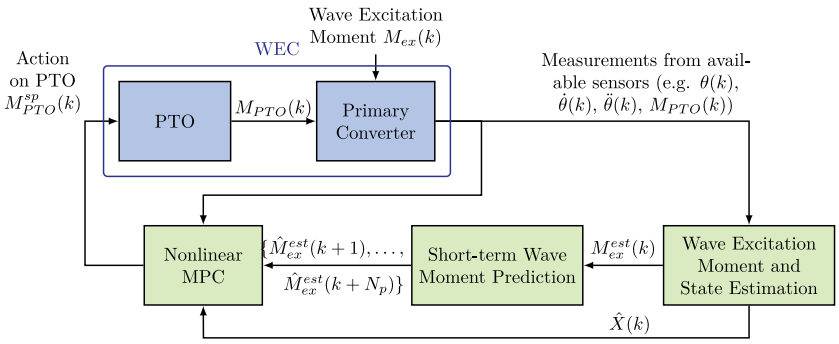

Fig. 7. IFPEN MPC system.

simulations of the iterative optimisation or, more rigorously, directly in MPC design, as part of the internal model.

As shown in Fig. 7, the wQP-MPC algorithm relies on the outputs of an algorithms for online estimation and short-term prediction of the wave excitation moment. The former uses measurements (or estimates) of the float angular displacement and velocity, as well as PTO moment, and is based on a Kalman filter coupled with a random-walk model of the variation of the wave excitation moment (Nguyen and Tona, 2017). It also provides an estimate of the state variables used by the MPC algorithm. The latter uses past and present values of wave excitation moment estimates (without any information from wave gauges), carrying out a multi-step-ahead prediction error minimisation via an adaptive bank of Kalman filters (AKF), recursive and easy to implement (Nguyen and Tona, 2018).

8.2. Controller tuning

The design model used for the wave and state estimator and for the wQP-MPC was a fourth-order space-state model, discretised respectively at 5 ms and 50 ms. Most nominal parameters were taken from the competition announcement paper (Ringwood et al., 2017), with the notable exception of an additional linear rotational damping term which the organisers had introduced in the simulator to match experimental measurements.

At the simulation stage, it was found that this design model could be improved, namely via a grey-box system identification procedure, but only marginally so for the most energetic waves. In view of the experimental implementation, it seemed sensible not to try matching the design model to the WEC-Sim simulation model, which could also show inaccuracies, but study its robustness instead.

A sensitivity analysis of power production to the choice of the damping term was carried out, as this parameter, corresponding to linearised viscous drag or mechanical friction (or a combination of both), is subject to significant uncertainty. It was found out that, also in the specific context of WECCCOMP, it is preferable to overestimate damping (Ringwood et al., 2020), rather than underestimating it. More precisely, the performance of an avg (P)-maximising or an EC-maximising wQP-MPC designed with the nominal damping value does not change significantly when applied to a WEC with a lower damping value. Conversely, underestimating damping in the design model was found detrimental to robustness in power production.

System identification results, from PTO excitation and wave excitation experiments, eventually proved that the nominal design model was accurate enough, especially for the most energetic sea states. All model and experimental transfer functions showed satisfactory agreement regarding the location of the peak response (governed by inertial and stiffness terms), while the response magnitude (governed by damping) differed across the three pairs of sea states, with smaller amplitudes for the data sets recorded in more energetic sea states. The identified damping values were smaller than the nominal one, but well inside the range where the robustness analysis had found minimal differences in power production.

Regarding the PTO dynamics, the experimental transfer function provided by the organisers in the simulator could not be included directly in the MPC internal model, because of the direct feedforward term. It was included in the iteratively simulated nominal plant model instead, and the weightings thus computed were chosen for the first-stage submission, yielding slightly better results (both on the linear nominal plant model and on the non-linear WECCCOMP simulator) than those computed by neglecting PTO dynamics. Experimentally, the PTO dynamics was found to be quite different from those included in the WECCCOMP simulator. The PTO reached the demanded torque very quickly, but with large spikes and high-frequency oscillations, probably due to stick–slip phenomena, the dynamics of which could not be captured by a linear model. 2nd and 1st-order transfer functions were identified with very small rise and settling times (both smaller than the MPC sampling time). Moreover, it was found that a unitary transfer function (an infinitely fast dynamics) would give the same fit as the PTO transfer function included in the WECCCOMP simulator.

Using the same design model as for wQP-MPC, the wave excitation moment estimator was tuned for all the sea states via the diagonal covariance matrices of the underlying Kalman filter. For the simulation stage, in the absence of noise, a quite aggressive tuning had been chosen to improve the fit with respect to the (nonlinear) wave excitation moment as computed by WEC-SIM. The experimental phase required a less aggressive tuning. Mimicking the procedure in simulation, data from free-float tests were used to run the wave moment estimator offline and compare the estimates to the values measured via the blocked-float experiments, thus allowing the validation of the less aggressive tuning obtained by reducing the weighting on the wave excitation moment computed by the random-walk model.

wQP-MPC was first tuned assuming perfect prediction. With a sample time of 50 ms, the prediction horizon h_p should be of at least 37 samples to cover the longest T_p among the evaluation sea-state. However, a shorter horizon of 25 samples (that is, 1.25 s) was chosen for design as it was found to work equally well. wQP-MPC performance showed little sensitivity to prediction accuracy; the adaptive Kalman filter bank was tuned for all the sea states at once (via diagonal covariance matrices, again) to provide accurate predictions for the first few future values, which sufficed to keep produced energy within 1%–2% of that obtained with perfect prediction.

An important parameter for MPC is M_{max}, the moment constraint on the PTO. For the expected range of motion, depending on θ, the linear force constraint $F_{max} = 60$ N maps onto a PTO moment situated between approximately 10 Nm and 12 Nm. Conservatively, a value of 10 Nm was chosen.

Other than h_p and M_{max}, no other wQP-MPC parameter needs manual tuning. The underlying QP matrices are directly computed from the weightings by the iterative optimisation procedure, performed in simulation with multiple runs of the linear nominal model on the chosen set of sea states. For the WECCCOMP submission, instead of

having a single set of weightings for all the sea states as in Nguyen et al. (2016), different sets were computed for sea-state pairs with the same T_p. A wave (or sea-state) "recognition" procedure was devised, based on the filtered estimate of the dominant frequency of wave excitation force, to automatically select and apply the appropriate set of parameters. In the context of the benchmark, the performance improvements over the use of a single set of weightings were only marginal (about 1% according to the simulation results), since the underlying optimisations were dominated by the two most energetic sea states. The real advantage in using this approach turned out to be the significant reduction in computation time, very convenient for the generation of multiple tuning sets.

Indeed, in order to limit on-the-fly or trial-and-error tuning during the 2.5 days of experiments, a great deal of preparation was carried out to anticipate as many scenarios as possible. More than 60 sets of weightings were generated for different combinations of settings (avg(P)/EC–maximising, by wave pairs/on all waves; with/without PTO dynamics), while all the other control parameters were given the same values as for the first stage, except for the wave moment estimator, which was detuned to cope with model mismatch and noise.

System identification and validation experiments performed during the first day of the tests showed that the nominal model used for design was accurate enough (with no strong case for taking into account PTO dynamics, though) and the performance of the detuned wave estimator was within acceptable bounds. Thus, after some debugging of the MPC code, Day 2 was essentially spent testing a subset of pre-computed weightings on the six repeatable realisations. Despite some uncertainties on computation procedures and on the actual energy content of the realisations, the results were found to be very close to those obtained in simulation on the linear design model (actually, about 10% better), with little difference in practical performance between avg(P)-maximising and EC-maximising weightings. This was considered encouraging enough to validate the experimental tuning process and use the validated set of weightings for the final evaluation.

A more comprehensive description of the experimental assessment of IFPEN solution is provided in Tona et al. (2020).

9. Competition results

For each sea state, the WECCCOMP competitors were instructed to evaluate their controller for a duration of $100T_p$ with a ramp time of $5T_p$, both for simulation and experiment. The first 25 s of the time records were discarded, allowing the start-up transients to disappear before calculating competition metrics. At the simulation stage, the WECCCOMP organisers reran all competitor submissions, compared the simulation results to submitted time series and recalculated the EC for each of the six sea states. This was completed to ensure the competitors' results were reproducible and could be used in other test cases, as required.

Note that, in this paper, the focus will be on the experimental (Section 9.2) and comparative simulation/experimental results, since the simulation results (including disaggregation into the various EC components) are described in detail in Ringwood et al. (2019). However, comparative experimental/simulation results are given in Section 9.3.

9.1. Controller comparisons

In this subsection, the salient point of each controller are compared, summarised in Table 4. A fundamental issue is the nature and fidelity of the WEC/PTO models employed, since all controllers are model based. For C2, no physical modelling is employed, with all system dynamic characteristics ascertained via data obtained from the system. In a commercial WEC design, this approach has the potential to save a considerable amount of time and effort, while also providing a controller based on real system data, potentially minimising modelling errors. In contrast, C1 and C2 use the (validated) mathematical model provided, though it should be noted that the validation was not performed under controlled conditions (Windt et al., 2021). However, while both C1 and C2 place value in further validating/tuning the model, C1 had insufficient time to complete this task.

In terms of controller choice, C1 and C3 opt for MPC-based controllers, which require an optimisation algorithm to be run in real time. In contrast, C2 uses a linear time-invariant (LTI) controller, the parametric structure of which (shown in (6)) is fixed, with the parameters determined using a Bayesian optimisation algorithm. Since an LTI controller, directly using the system velocity measurement, in a feedback configuration, is employed, there is no need to estimate the excitation force, nor forecast it (as with the controller of C1 and C3). Therefore, the C2 controller belongs to the class of approximate Complex Conjugate (ACC) controllers, while the C1 and C3 controllers implement Approximate Velocity Tracking (AVT) (Ringwood et al., 2023). There is no doubt that the simpler controller of C2 is partly responsible for the inferior performance, in that the complex conjugate can only be achieved at a single frequency, while all 6 sea states contain broadband components. One other important issue is that ACC controllers have no easy way to take account of system constraints.

Though provided, only C1 used up-wave measurements. In an open-ocean setting, the value of up-wave measurements may be diminished (Paparella et al., 2014), since multiple wave directions may be encountered, while unidirectional waves only are present in the wave tank for this test. Mérigaud and Ringwood (2018) gives some useful results regarding what accuracy may be achieved using up-wave measurement, in poly-directional wave conditions.

Crucially, only C3 tuned the controller performance function weights, which may help to explain the superior performance of the C3 controller. However, in an open ocean scenario, it is questionable whether all the sea states occurring at a particular wave site (possibly articulated using a scatter plot) could be considered for tuning, and some technique to correctly identify the current sea state would also be necessary.

Perhaps the most striking conclusion from the comparison of controllers is the difference in performance between the MPC and the LTI controller of C2. It has been somewhat of an open question as to the value of the significant extra implementation complexity of MPC, or MPC-like controllers, which require on-line optimisation, compared to simple (perhaps more intuitive) controllers, being the subject of a number of other studies (Faedo et al., 2023, 2020). That MPC is robust enough to deal with some modelling inaccuracies (though C3 did an amount of model tuning) and is implementable in real time on a small scale WEC, where the sampling period requirements are more onerous than for full scale, is testament to the potential for MPC WEC control at commercial scale.

9.2. Experimental results

Using the WEC system as shown in Fig. 2, with the controller hardware as shown in Fig. 4, each competitor was given some assistance in implementing their controller. Following this commissioning phase, each competitor ran their controller for three realisations of each of the sea states, documented in Table 2, in order to get statistically significant results. By way of example, Figs. 8 to 10 show the time series evolution of the device angular displacement, and moment, along with the corresponding constraints, for Competitors 1 (C1) to 3 (C3), respectively.

From Figs. 8 to 10, it is noteworthy that, despite the sea state (and therefore excitation force) being identical for each of the three cases, the control moments and displacements show significantly different characteristics, particularly in relation to the control moment. For C1, the constraints are generously satisfied, while some excesses in negative control moment are present in the trace for C2. For C3, it could be said that the control space is fully exploited, with some minor excursions beyond the constraints. To assist in this comparison, the resulting time

Table 4
Controller comparison table.

Competitor	Model refinement	Controller	Estimation	Forecasting measurement	Used up-wave measurements	Sea-state handling	Constraint
C1	No time	MPC	Yes (F_e and state)	Yes	Yes	No	Yes
C2	Sys ID	LTI	Sim only	No	No	No	No
C3	Yes	MPC	Yes (F_e and state)	Yes	No	Yes	Yes

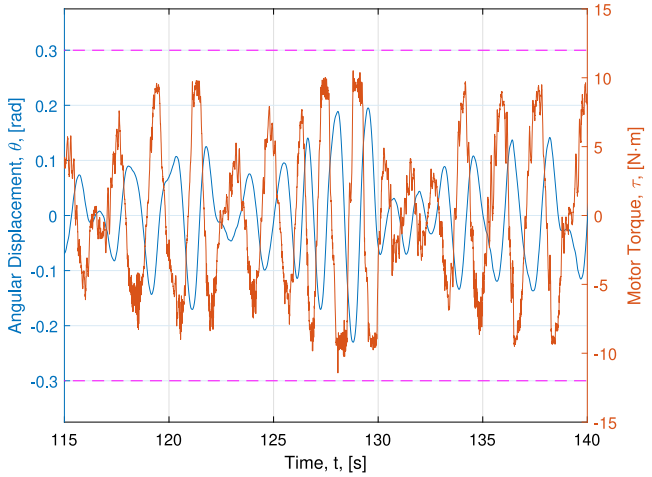

Fig. 8. Example time series, Sea State 3, Realisation 1, for Competitor 1 with magenta dashed dotted lines representing minimum and maximum thresholds.

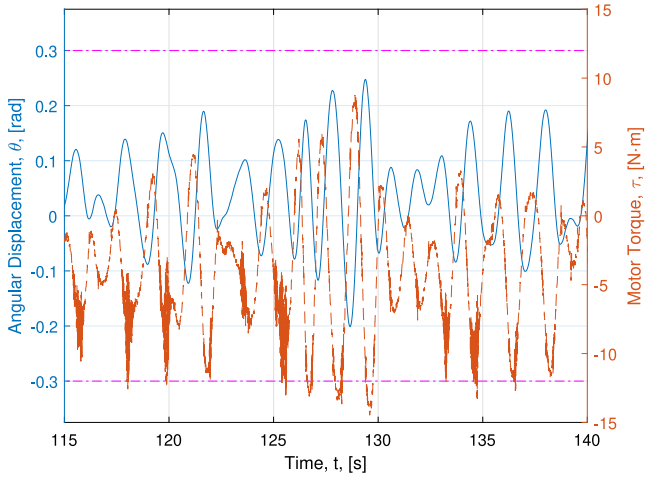

Fig. 9. Example time series, Sea State 3, Realisation 1, for Competitor 2 with magenta dashed dotted lines representing minimum and maximum thresholds.

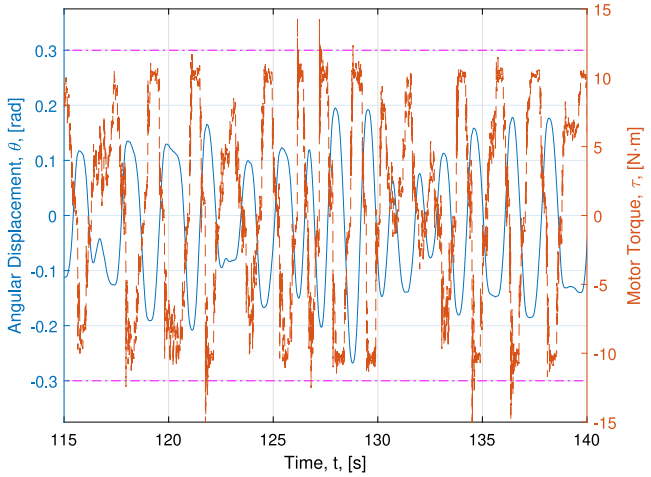

Fig. 10. Example time series, Sea State 3, Realisation 1, for Competitor 3 with magenta dashed dotted lines representing minimum and maximum thresholds.

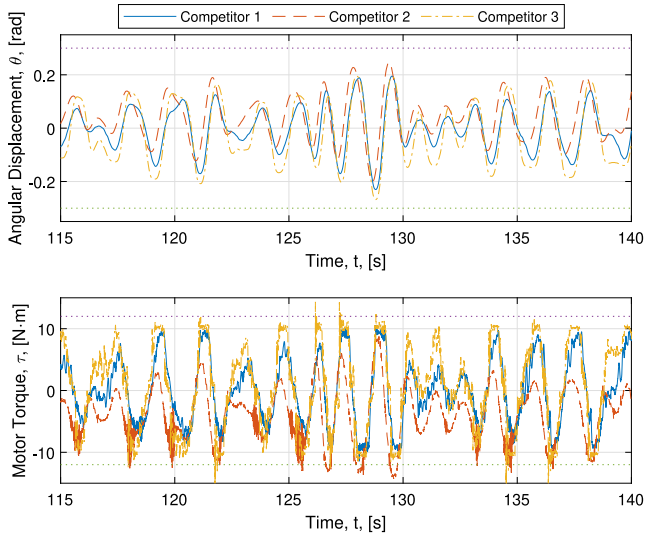

Fig. 11. Example time series, Sea State 3, Realisation 1, for all Competitors with dotted lines representing minimum and maximum thresholds.

histories of angular displacement and motor torque for each competitor are superimposed on the same plots, as shown in Fig. 11, that highlight the previous observations.

Fig. 12 shows the various scores achieved by each competitor on the different sea states (recalling that the EC is averaged across three sea state realisations). Relatively consistent results, in terms of ranking of competitors, are achieved across each of the six sea states and we note that Sea State 6 is, by and large, a survival sea state. However, C3 achieves a consistently better EC than C1 and C2 and is the competition winner. Of particular note, in Fig. 12 is the net negative EC for Competitor 2, for Sea States 1 and 4. This is explained by the relative contributions of each component to the EC in (2), namely that: $2 + \frac{|f|_{98}}{F_{max}} + \frac{|z|_{98}}{Z_{max}} < \frac{\text{avg}|P|}{|P|_{98}}$ for those particular cases, illustrated also in Fig. 14. Specifically, net negative energy can be produced (i.e. net energy *consumption* can occur in cases when mismatch is present between the controller model and the real system, as articulated in Ringwood et al. (2020) and Bacelli et al. (2015).

The breakdown of EC components in Eq. (2) achieved by each competitor, averaged across sea-state realisations, is shown in Figs. 13 to 15. For example, the overall competition winner, C3, achieved the best average power production figures, but competitor C2 scored best in terms of average-to-peak power (avg $|P|$ / $|P|_{98}$) scores. The strength of C1's controller was in producing minimal displacement constraint violations ($|z|_{98}$ / Z_{max}).

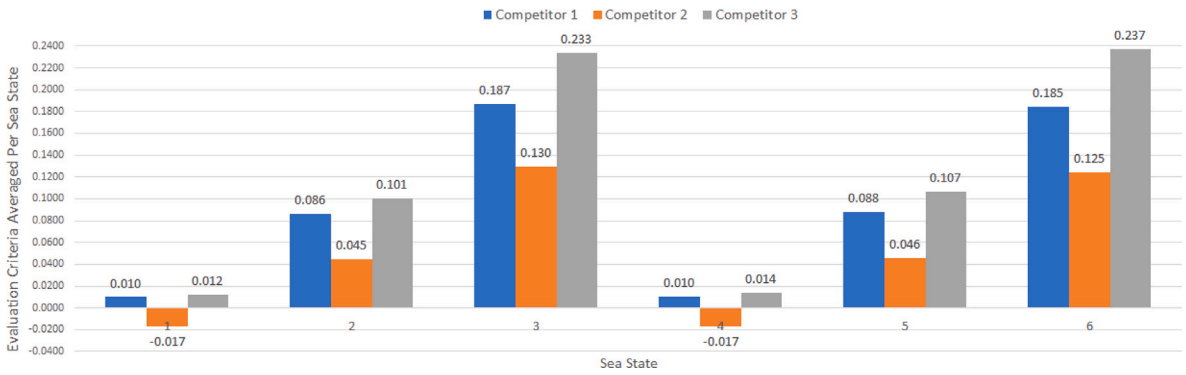

Fig. 12. Experimental results for different competitors, across the different sea states.

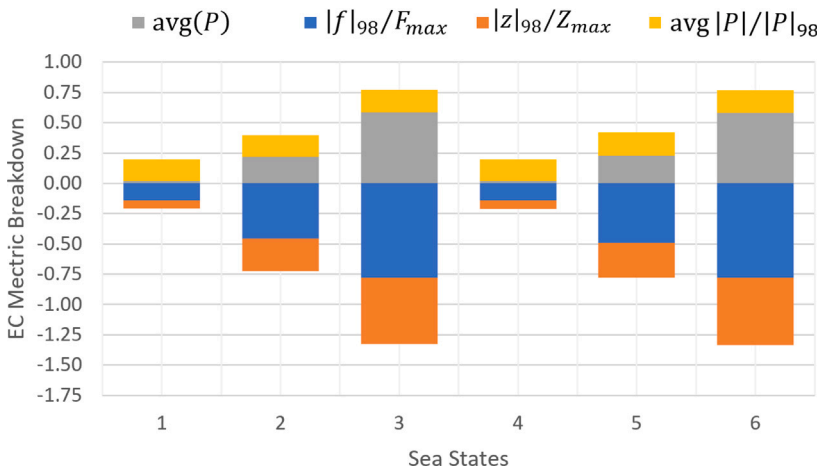

Fig. 13. Breakdown in EC components for Competitor 1. Note that $\text{avg}(P)$ and $\text{avg}|P|/|P|_{98}$ are positive contributors to EC, while $|f|_{98}/F_{max}$ and $|z|_{98}/Z_{max}$ are negative contributors, as indicated.

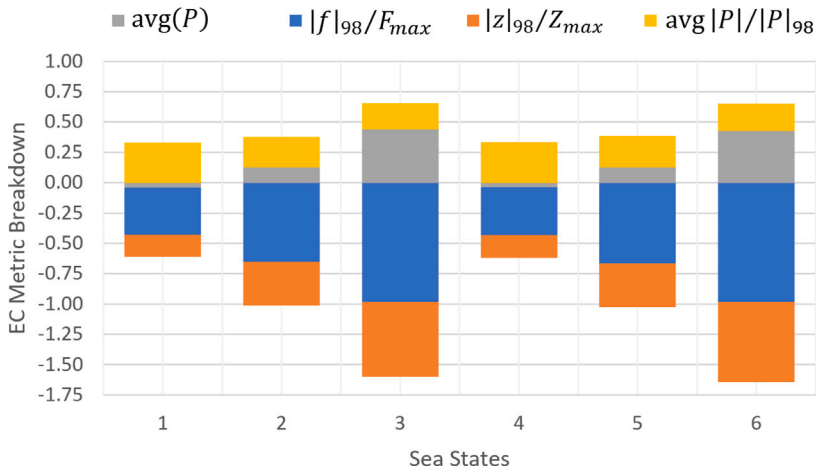

Fig. 14. Breakdown in EC components for Competitor 2. Note that $\text{avg}(P)$ and $\text{avg}|P|/|P|_{98}$ are positive contributors to EC, while $|f|_{98}/F_{max}$ and $|z|_{98}/Z_{max}$ are negative contributors, as indicated.

9.3. Comparative simulation/experimental results

It is interesting to compare the experimental results to those achieved for the simulation stage of the competition, and this comparison is shown in Table 5. One remarkable feature is the consistency in the relative ranking of competitors across both simulation and experimentation. However, one unexpected feature is that, for C3, the EC achieved on the experimental test actually exceeds that for the simulation test, while the more expected deterioration in simulation → experimental EC is observed for C1 and C2, though the experimental results for C1 were within 2% of those achieved in simulation. Table 5 gives a quantitative measure of the EC performance for each competitor, in both relative and absolute terms. As highlighted in Section 9.1, C1 and C3 utilise MPC controllers, compared to the LTI controller of C2, which helps to explain the significant discrepancy between the EC values of C1, C3 and C2.

Further insight into the operation of each controller may be gleaned from Tables 6 to 8, which show the minima, maxima, and standard

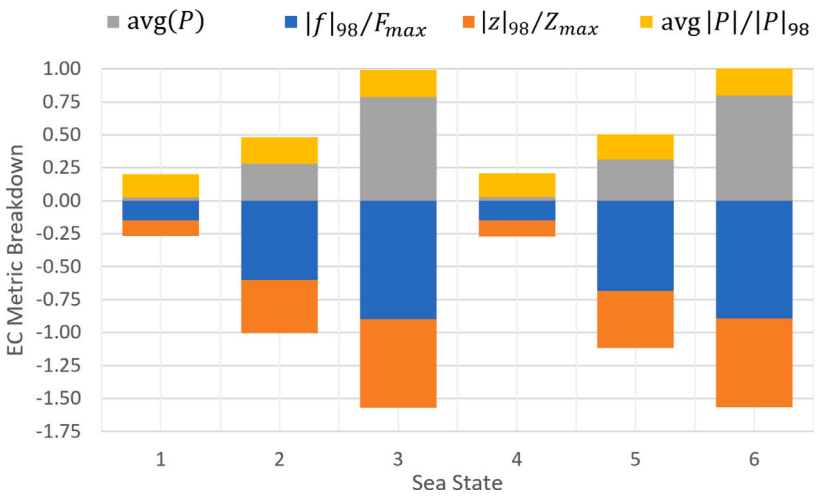

Fig. 15. Breakdown in EC components for Competitor 3. Note that avg (P) and avg $|P|/|P|_{98}$ are positive contributors to EC, while $|f|_{98}/F_{max}$ and $|z|_{98}/Z_{max}$ are negative contributors, as indicated.

Table 5
EC scores for simulation and experimental evaluation.

Entry	Simulation		Experimental	
	Aver. EC	Norm EC	Aver. EC	Norm. EC
C3	0.0975	1.0000	0.1174	1.0000
C1	0.0963	0.9877	0.0943	0.8038
C2	0.0826	0.8472	0.0517	0.4408

deviations of the EC components, f/F_{max} and z/Z_{max}, and the overall power efficiency P/P_w, for each sea state. The following can be ascertained:

- Controllers C1 and C3 tend to exploit the maximum force range to a greater extent, compared to C2, while C2 generally has a larger operational space, in terms of displacement.
- The statistical measures on P/P_w particularly show the excessive amount of reactive power being utilised by C2, indicated by the negative (min) P/P_w values (see especially SS1 and SS4), and contributing to the overall average negative EC values for SS1 and SS4 shown in Fig. 12. This is typically due to a mismatch between the system and controller, perhaps related to the fixed LTI controller structure of C2.
- The Std P/P_w values show good consistency in performance across different sea states for C1 and C3, indicating that the system efficiency (% of captured wave power) is not effected by sea state changes, while C2 has significantly larger Std values.

10. Conclusions

Though limited time was available to each team for experimentation, each team managed to get an operational controller, which suggests that the implementation (design was performed off-line) of MPC-type controllers for wave energy systems is not too onerous. Nevertheless, all teams remarked on the tight implementation schedule, and could have used extra time for model and controller tuning. However, the simpler LTI controller of C2 presents a more straightforward commissioning procedure, especially since the controller can be determined directly from system data, avoiding the need for physical modelling. However, the better performance achieved by C1 and C3 suggest that the extra effort of an MPC controller, based on a physical system model, is worth it. In particular, the average negative power achieved in S1 and S4 by C2 are concerning, with the excessive reactive power flow levels suggesting that there is mismatch between the real system and that which the controller believes generated the data.

One main overall conclusion is that the control results were broadly consistent from simulation to implementation, suggesting that the linear (validated) hydrodynamic and PTO models provided were appropriate, although most competitors took the opportunity to perform some additional tests on the experimental system.

Some other specific conclusions:

- A number of competitors, for the experimental and simulation cases, tuned the controller to each individual sea state using some off-line procedure. The degree to which this can be done in a practical/operational scenario is questionable in (a) filling in a look-up table and (b) recognising a sea state to allow parameter scheduling. To this end, competitor team C3 implemented a 'wave recognition' feature. Such experience might inform the specification of any future WEC control competitions.
- Some algorithms use up-wave measurements (C1) while others do not (C2). There appears to be little discrepancy between the quality of excitation force estimates and maybe suggests that the added expense of up-wave can be eliminated (consistent with Paparella et al. (2014)), while also avoiding the issue of wave directionality.
- Similarly to many other WEC control designs (e.g. Paparella et al. (2016)), the model is often 'tuned' by identifying a linear damping term, which is often where uncertainty lies. Interestingly, the sensitivity to damping parameter errors is considered by competitor C3, bearing in mind that different control topologies will have different sensitivity to various hydrodynamic modelling error types (Ringwood et al., 2020). In particular, the importance of not underestimating damping is highlighted.
- In order to maximise the value of tank testing time, some competitors (e.g. C3) precomputed controller settings for a range of weighting values, which avoided the need to run computationally expensive (even if off-line) optimisation routines during the active tank testing period.
- The experimental process employed by each competitor differed slightly, but this reported information should be of benefit to practitioners wishing to implement WEC controllers, whether for experimental testing or operational use. No doubt, the restricted time available for implementation/testing impacted the adopted procedure, though some advice is given as to how additional time could be usefully employed.

It is hoped that the information reported in this paper may help to inform both the research and practice of WEC control design, while it also serves to inform the design of future WEC control benchmark

Table 6
Minimum, maximum and standard deviation statistics of the time-histories for force, displacement, and electrical power for Competitor 1.

Sea state	f/F_{max}			z/Z_{max}			P/P_w		
	Min	Max	Std	Min	Max	Std	Min	Max	Std
1	−0.187	0.223	0.057	−0.075	0.080	0.027	−0.488	1.598	0.192
2	−0.601	0.626	0.194	−0.334	0.337	0.113	−0.287	1.009	0.135
3	−0.905	0.901	0.391	−0.782	0.771	0.244	−0.309	1.120	0.135
4	−0.225	0.218	0.059	−0.082	0.097	0.029	−0.652	1.797	0.208
5	−0.662	0.677	0.197	−0.395	0.370	0.118	−0.283	1.193	0.134
6	−0.895	0.896	0.392	−0.799	0.691	0.238	−0.276	0.877	0.114

Table 7
Minimum, maximum and standard deviation statistics of the time-histories for force, displacement, and electrical power for Competitor 2.

Sea state	f/F_{max}			z/Z_{max}			P/P_w		
	Min	Max	Std	Min	Max	Std	Min	Max	Std
1	−0.495	−0.107	0.045	0.002	0.214	0.035	−4.413	4.261	1.328
2	−1.096	0.204	0.166	−0.214	0.443	0.114	−0.571	1.608	0.231
3	−1.232	0.752	0.325	−0.660	0.942	0.257	−0.485	0.902	0.147
4	−0.509	−0.082	0.051	−0.008	0.229	0.040	−4.646	4.413	1.393
5	−1.235	0.300	0.174	−0.227	0.491	0.110	−0.658	1.650	0.206
6	−1.241	0.776	0.315	−0.777	0.955	0.256	−0.461	0.940	0.134

Table 8
Minimum, maximum and standard deviation statistics of the time-histories for force, displacement, and electrical power for Competitor 3.

Sea state	f/F_{max}			z/Z_{max}			P/P_w		
	Min	Max	Std	Min	Max	Std	Min	Max	Std
1	−0.249	0.226	0.058	−0.145	0.084	0.040	−1.001	2.501	0.257
2	−0.882	0.794	0.248	−0.527	0.441	0.177	−0.988	1.518	0.201
3	−1.527	1.316	0.536	−0.912	0.761	0.360	−0.410	1.204	0.166
4	−0.228	0.217	0.058	−0.152	0.098	0.043	−0.772	2.197	0.261
5	−0.874	0.894	0.263	−0.568	0.499	0.182	−1.018	1.694	0.209
6	−1.442	1.206	0.534	−0.949	0.773	0.349	−0.326	1.083	0.140

problems. One area for focus is the evaluation criterion used, since it was found that the competition result was relatively sensitive to the EC structure. However, aiming for an EC which is representative of LCoE, while also being computable in the short term, is a compromise that deserves further exploration.

This study has some limitations, which limit the generality of any conclusions. Specifically, the study focuses on a point-absorber WEC and, while this representative of a relatively wide range of WEC systems, the diversity of WEC designs (which include oscillating wave surge converters (OWSC), oscillating water columns, connected structures, etc.) and the many different prototypes proposed (Guo and Ringwood, 2021) preclude any entirely generic conclusions. Furthermore, the use of a point absorber may bias the effectiveness (or otherwise) of any controller comparison. In particular, since a point absorber is a resonant device, it responds well to aggressive reactive control. For example, an OWSC, which has a less resonant but more broadband response, may react differently to the range of controllers presented in this study, or even respond well to (economical) resistive control. Finally, the range of controllers compared in this study was limited. However, given that this prototype rig has been, and is likely to be, utilised by other control researchers, the set of comparable results has the capability to broaden significantly.

As a benchmark problem itself, the WECCCOMP system has, to date, had some moderate success in promoting both simulation-based (Tang et al., 2020; Guerrero-Fernández et al., 2022) and experimental (García-Violini et al., 2021; Faedo et al., 2023; García-Violini et al., 2023) assessment of WEC controllers. We hope that the WECCCOMP benchmark will continue to be of service to the wave energy community: Online resources for simulation are maintained by Sandia/NREL (see WECCCOMPGithub (2018)) and the WECCCOMP organisers would be delighted to receive feedback and comments regarding WECCCOMP, and possible future benchmark competitions.

CRediT authorship contribution statement

John V. Ringwood: Conceptualisation, Writing – original draft, Writing – review & editing, Supervision, Funding acquisition, Project administration. **Nathan Tom:** Conceptualisation, Writing – original draft, Writing – review & editing, Funding acquisition. **Francesco Ferri:** Conceptualisation, Writing – original draft, Writing – review & editing, Software, Funding acquisition. **Yi-Hsiang Yu:** Conceptualisation, Writing – original draft, Writing – review & editing. **Ryan G. Coe:** Conceptualisation, Writing – original draft, Writing – review & editing. **Kelley Ruehl:** Conceptualisation, Writing – original draft, Writing – review & editing. **Giorgio Bacelli:** Conceptualisation, Writing – original draft, Writing – review & editing. **Shuo Shi:** Conceptualisation, Methodology, Software, Writing – original draft, Writing – review & editing. **Ron J. Patton:** Conceptualisation, Methodology, Writing – original draft, Writing – review & editing, Supervision. **Paolino Tona:** Conceptualisation, Methodology, Software, Writing – original draft, Writing – review & editing, Supervision. **Guillaume Sabiron:** Conceptualisation, Methodology, Software, Writing – review & editing. **Alexis Merigaud:** Conceptualisation, Methodology, Software, Writing – review & editing. **Bradley A. Ling:** Conceptualisation, Methodology, Software, Writing – original draft, Writing – review & editing. **Nicolas Faedo:** Conceptualisation, Writing – original draft, Writing – review & editing, Supervision.

Declaration of competing interest

The authors declare the following financial interests/personal relationships which may be considered as potential competing interests: John V. Ringwood reports financial support was provided by Science Foundation Ireland. John V. Ringwood reports financial support was

provided by European Commission. Kelley Ruehl, Nathan Tom, Yi-Hasiany Yu, Giorgio Bacelli, Ryan Coe reports financial support was provided by US Department of Energy. Nicolas Faedo reports financial support was provided by Science Foundation Ireland.

Data availability

Data will be made available on request.

Acknowledgment

This work was supported by Science Foundation Ireland under Grant No. SFI/13/IA/1886 and through the Research Centre for Energy, Climate and Marine (MaREI) under Grant No. 12/RC/2302_P2. The research leading to these results has also received funding from the European Union Horizon 2020 Framework Programme (H2020) under Marinet 2 Grant No. 731084. This work was co-authored by the National Renewable Energy Laboratory, operated by Alliance for Sustainable Energy, LLC,for the U.S. Department of Energy (DOE) under Contract No. DE-AC36-08GO28308. Funding was also provided by the U.S. Department of Energy, USA, Office of Energy Efficiency and Renewable Energy, USA, Water Power Technologies Office, USA. The views expressed in the article do not necessarily represent the views of the DOE or the U.S. Government. The U.S. Government retains and the publisher, by accepting the article for publication, acknowledges that the U.S. Government retains a nonexclusive, paid-up, irrevocable, worldwide licence to publish or reproduce the published form of this work, or allow others to do so, for U.S. Government purposes. Sandia National Laboratories is a multimission laboratory managed and operated by National Technology & Engineering Solutions of Sandia, LLC, a wholly owned subsidiary of Honeywell International Inc., for the U.S. Department of Energy's National Nuclear Security Administration under contract DE-NA0003525.

References

Abdelrahman, M., Patton, R., 2019. Observer-based unknown input estimator of wave excitation force for a wave energy converter. IEEE Trans. Control Syst. Technol. 28 (6), 2665–2672.

Bacelli, G., Genest, R., Ringwood, J.V., 2015. Nonlinear control of flap-type wave energy converter with a non-ideal power take-off system. Annu. Rev. Control 40, 116–126.

Bacelli, G., Nevarez, V., Coe, R.G., Wilson, D.G., 2019. Feedback resonating control for a wave energy converter. IEEE Trans. Ind. Appl. 56 (2), 1862–1868.

Bjerrum, A., 2008. The wave star energy concept. In: 2nd International Conference on Ocean Energy. Brest, France, 15-17 Oct 2008.

Brekken, T.K., 2011. On model predictive control for a point absorber wave energy converter. In: *PowerTech*. Trondheim, Norway, pp. 1–8.

Coe, R.G., Bacelli, G., Wilson, D.G., Abdelkhalik, O., Korde, U.A., Robinett, III, R.D., 2017. A comparison of control strategies for wave energy converters. Int. J. Mar. Energy 20, 45–63.

Cummins, W., 1962. The Impulse Response Function and Ship Motions. David Taylor Model Dasin (DTNSRDC) Report, David Taylor Model Dasin (DTNSRDC).

Faedo, N., García-Violini, D., Peña-Sanchez, Y., Ringwood, J.V., 2020. Optimisation-vs. non-optimisation-based energy-maximising control for wave energy converters: A case study. In: European Control Conference. ECC, St. Petersburg, IEEE, pp. 843–848.

Faedo, N., Peña-Sanchez, Y., Garcia-Violini, D., Ferri, F., Mattiazzo, G., Ringwood, J.V., 2023. Experimental assessment and validation of energy-maximising moment-based optimal control for a prototype wave energy converter. Control Eng. Pract. 133, 105454.

Ferri, F., Ambühl, S., Fischer, B., Kofoed, J.P., 2014. Balancing power output and structural fatigue of wave energy converters by means of control strategies. Energies 7 (4), 2246–2273.

Fusco, F., Ringwood, J.V., 2010. Short-term wave forecasting for real-time control of wave energy converters. IEEE Trans. Sustain. Energy 1 (2), 99–106.

Fusco, F., Ringwood, J.V., 2011. A model for the sensitivity of non-causal control of wave energy converters to wave excitation force prediction errors. In: Proceedings of the 9th European Wave and Tidal Energy Conference. EWTEC, Southampton.

Fusco, F., Ringwood, J.V., 2012. A study of the prediction requirements in real-time control of wave energy converters. IEEE Trans. Sustain. Energy 3 (1), 176–184.

García-Violini, D., Peña-Sanchez, Y., Faedo, N., Ferri, F., Ringwood, J.V., 2023. A broadband time-varying energy maximising control for wave energy systems (LiTe-Con+): Framework and experimental assessment. IEEE Trans. Sustain. Energy (Early Access).

García-Violini, D., Peña-Sanchez, Y., Faedo, N., Windt, C., Ferri, F., Ringwood, J.V., 2021. Experimental implementation and validation of a broadband LTI energy-maximizing control strategy for the wavestar device. IEEE Trans. Control Syst. Technol. 29 (6), 2609–2621.

Guerrero-Fernández, J.L., Tom, N.M., Rossiter, J.A., 2022. Nonlinear model predictive control based on real-time iteration scheme for wave energy converters using WEC-Sim. In: ASMA Intl. Conf. on Offshore Mechanics and Arctic Eng., Vol. 85932. OMAE, Hamburg, p. V008T09A076.

Guo, B., Ringwood, J.V., 2021. A review of wave energy technology from a research and commercial perspective. IET Renew. Power Gener. 15 (14), 3065–3090.

Hals, J., Falnes, J., Moan, T., 2011. A comparison of selected strategies for adaptive control of wave energy converters. J. Offshore Mech. Arct. Eng. 133 (3), 031101.

Lee, C., Newman, J., 2016. WAMIT user manual version 7.2.

Ling, B.A., 2019. Development of a model predictive controller for the wave energy converter control competition. In: ASME Intl. Conf. on Offshore Mechanics and Arctic Engineering, Volume 10: Ocean Renewable Energy. Glasgow.

Ling, B., Batten, B., 2015. Real time estimation and prediction of wave excitation forces on a heaving body. In: *Proc. ASME 34th Intl. Conf. on Ocean, Offshore and Arctic Engineering, St. John's*. pp. V009T09A017–V009T09A017.

Ling, B.A., Bosma, B., Brekken, T.K., 2019. Experimental validation of model predictive control applied to the Azura wave energy converter. IEEE Trans. Sustain. Energy 11 (4), 2284–2293.

Mérigaud, A., Ringwood, J.V., 2018. Incorporating ocean wave spectrum information in short-term free-surface elevation forecasting. IEEE J. Ocean. Eng. 44 (2), 401–414.

Neary, V.S., Lawson, M., Previsic, M., Copping, A., Hallett, K.C., Labonte, A., Rieks, J., Murray, D., et al., 2014. Methodology for Design and Economic Analysis of Marine Energy Conversion (MEC) Technologies. Technical Report SAND2014-9040.

Nguyen, H.-N., Sabiron, G., Tona, P., Kramer, M.M., Sanchez, E.V., 2016. Experimental validation of a nonlinear MPC strategy for a wave energy converter prototype. In: ASME 35th Intl. Conference on Ocean, Offshore and Arctic Engineering. American Society of Mechanical Engineers, V006T09A019.

Nguyen, H.-N., Tona, P., 2017. Wave excitation force estimation for wave energy converters of the point absorber type. IEEE Trans. Control Syst. Technol. 26 (6), 2173–2181.

Nguyen, H.-N., Tona, P., 2018. Short-term wave force prediction for wave energy converter control. Control Eng. Pract. 75, 26–36.

Paparella, F., Bacelli, G., Paulmeno, A., Mouring, S.E., Ringwood, J.V., 2016. Multi-body modelling of wave energy converters using pseudo-spectral methods with application to a three-body hinge-barge device. IEEE Trans. Sustain. Energy 7 (3), 966–974.

Paparella, F., Monk, K., Winands, V., Lopes, M., Conley, D., Ringwood, J.V., 2014. Up-wave and autoregressive methods for short-term wave forecasting for an oscillating water column. IEEE Trans. Sustain. Energy 6 (1), 171–178.

Ringwood, J.V., Bacelli, G., Fusco, F., 2014. Energy-maximizing control of wave-energy converters: The development of control system technology to optimize their operation. IEEE Control Syst. 34 (5), 30–55.

Ringwood, J., Ferri, F., Ruehl, K.M., Yu, Y.-H., Coe, R., Bacelli, G., Weber, J., Kramer, M., 2017. A competition for WEC control systems. In: Proc. 12th European Wave and Tidal Conference. EWTEC, Cork, Ireland.

Ringwood, J., Ferri, F., Tom, N.M., Ruehl, K., Faedo, N., Bacelli, G., Yu, Y.-H., Coe, R., 2019. The wave energy converter control competition: Overview. In: Prof. 39th Intl. Conf on Offshore and Arctic Engineering. p. 95216.

Ringwood, J.V., Mérigaud, A., Faedo, N., Fusco, F., 2020. An analytical and numerical sensitivity and robustness analysis of wave energy control systems. IEEE Trans. Control Syst. Technol. 28 (4), 1337–1348.

Ringwood, J.V., Mérigaud, A., Faedo, N., Fusco, F., 2020. An analytical and numerical sensitivity and robustness analysis of wave energy control systems. IEEE Trans. Control Syst. Technol. 28 (4), 1337–1348.

Ringwood, J.V., Zhan, S., Faedo, N., 2023. Empowering wave energy with control technology: Possibilities and pitfalls. Annu. Rev. Control.

Ruehl, K., Yu, Y.-H., M., L., Michelen, C., 2014. Preliminary verification and validation of WEC-SIM, an open-source wave energy converter design tool. In: Proc. of the ASME 33rd International Conference on Ocean, Offshore and Arctic Engineering. OMAE.

Shi, S., Patton, R.J., Abdelrahman, M., Liu, Y., 2019. Learning a predictionless resonating controller for wave energy converters. In: Proc. Intl.L Conf. on Offshore Mechanics and Arctic Eng. Glasgow.

Shi, S., Patton, R.J., Liu, Y., 2018. Short-term wave forecasting using Gaussian process for optimal control of wave energy converters. IFAC-PapersOnLine 51 (29), 44–49.

Starrett, M., So, R., Brekken, T., McCall, A., 2015. Increasing power capture from multibody wave energy conversion systems using model predictive control. In: *IEEE Conf. on Technologies for Sustainability*. SusTech, pp. 20–26.

Tang, Y., Huang, Y., Lindbeck, E., Lizza, S., VanZwieten, J., Tom, N., Yao, W., 2020. WEC fault modelling and condition monitoring: A graph-theoretic approach. IET Electr. Power Appl. 14 (5), 781–788.

Tom, N., Ruehl, K., Ferri, F., 2018. Numerical Model Development and Validation for the WECCCOMP Control Competition. In: Proc. 38th Intl. Conf. on Ocean, Offshore and Arctic Engineering. OMAE, Madrid, Spain.

Tona, P., Sabiron, G., Nguyen, H.-N., Mérigaud, A., Ngo, C., 2020. Experimental assessment of the IFPEN solution to the WEC control competition. In: ASME 39th Intl. Conference on Ocean, Offshore and Arctic Engineering. p. V009T09A023.

WEC-Sim, 2018. WEC-Sim - Wave Energy Converter SIMulator. http://wec-sim.github.io/WEC-Sim/. (Accessed January 2018).

WEC-Sim-Github, 2018. WEC-Sim GitHub Repository v3.0. https://github.com/WEC-Sim/WEC-Sim. (Accessed January 2018).

WECCCOMPGithub, 2018. WECCCOMP GitHub Repository. https://github.com/WEC-Sim/WECCCOMP. (Accessed 15 December 2018).

Windt, C., Faedo, N., Penalba, M., Dias, F., Ringwood, J.V., 2021. Reactive control of wave energy devices–the modelling paradox. Appl. Ocean Res. 109, 102574.